Determining the neutron skin thickness by relativistic semi-isobaric collisions

Qi Liu,[1] Shujun Zhao,[1] Hao-jie Xu,[2,3,4,*] and Huichao Song[1,5,6,†]
[1]*School of Physics, Peking University, Beijing 100871, China*
[2]*School of Science, Huzhou University, Huzhou, Zhejiang 313000, China*
[3]*Strong-Coupling Physics International Research Laboratory (SPiRL), Huzhou University, Huzhou, Zhejiang 313000, China*
[4]*Shanghai Research Center for Theoretical Nuclear Physics, NSFC and Fudan University, Shanghai 200438, China*
[5]*Center for High Energy Physics, Peking University, Beijing 100871, China*
[6]*Collaborative Innovation Center of Quantum Matter, Beijing 100871, China*

(Received 6 November 2023; accepted 9 February 2024; published 18 March 2024)

The neutron skin thickness of the benchmark nucleus ^{208}Pb is crucial for our understanding of the equation of state of nuclear matter. In this paper, we discuss the effect of the neutron skin on the flow ratio observables in the semi-isobaric collisions ^{208}Pb + ^{208}Pb and ^{197}Au + ^{197}Au using IEBE-VISHNU hydrodynamic simulations. Our results suggest that ^{208}Pb and ^{197}Au should have the same magnitude of neutron skin thickness to describe the anisotropic flow ratios between the semi-isobaric systems. Our method provides an unconventional way to determine the neutron skin with the existing relativistic heavy ion collision data.

DOI: 10.1103/PhysRevC.109.034912

I. INTRODUCTION

The equation of state (EoS) of nuclear matter governs the general properties of the nuclear force over several orders of magnitude, from nuclei to neutron stars [1–4]. The symmetry energy in the EoS encodes the energy associated with the neutron-proton asymmetry. Measurements of the neutron skin thickness $\Delta r_{\rm np}$ can provide valuable information about the nuclear symmetry energy [5–12]. The neutron skin of the benchmark nuclei ^{208}Pb ($\Delta r_{\rm np} = 0.28 \pm 0.07$ fm) and ^{48}Ca ($\Delta r_{\rm np} = 0.121 \pm 0.026 \pm 0.024$ fm) were recently measured by the lead radius experiment PREX-II and the calcium radius experiment CREX with parity violating electron nucleus scattering processes [13,14]. Based on the energy density functional calculations, the PREX-II data lead to a stiff EoS, while the CREX data favor a softer EoS [15]. These results challenged our current understanding of the EoS of nuclear matter, which led to extensive studies in low energy nuclear physics in the past two years [16,17]. In general, the measurement of the mass radii can be used directly to determine the neutron skin thickness of such nuclei, given that their charge radii can be accurately measured. The photoproduction of neutral ρ mesons has been found to be sensitive to the mass radii of the colliding nuclei, and this method has been applied in relativistic heavy ion collisions [18,19]. The neutron skin of ^{197}Au ($\Delta r_{\rm np} = 0.17 \pm 0.03 \pm 0.08$ fm) has been measured by the STAR Collaboration with the $\rho^0 \to \pi^+\pi^-$ photoproduction method in ultraperipheral Au + Au collisions (UPCs) at $\sqrt{s_{NN}} = 200$ GeV [19].

Recently, more unconventional methods have been proposed for neutron skin thickness measurements in relativistic heavy ion collisions [20–29]. In heavy ion collisions at top energies available at the BNL Relativistic Heavy Ion Collider (RHIC) and the CERN Large Hadron Collider (LHC), the quark gluon plasma (QGP), a decoupled phase of quarks and gluons, has been created [30–34]. The QGP can be successfully described by relativistic hydrodynamics simulations with a small specific shear viscosity [35–41]. It was also found that the final state observables, such as multiplicity, mean transverse momentum, and anisotropic flow, are intrinsically related to the initial state and thus sensitive to the structure of the colliding nuclei [38,39,42,43]. These observables are subject to less uncertainty from the strong interactions in quantum chromodynamic theory than the observables in low-energy hadronic collisions. However, it is difficult to directly distinguish the subtle nuclear structure effects in a single collision system due to the uncertainties in the bulk properties of the QGP evolution, although some efforts have been made recently [29,43]. The RHIC isobaric runs with $^{96}_{40}$Zr + $^{96}_{40}$Zr and $^{96}_{44}$Ru + $^{96}_{44}$Ru collisions at $\sqrt{s_{NN}} = 200$ GeV, originally designed to search for the chiral magnetic effect (CME), provide unique opportunities to probe the nuclear structures of the colliding nuclei from the early stages [20–28,44–46]. This is because the uncertainties from the bulk properties of the QGP can be significantly reduced by the observable ratios between the two collision systems [45,47]. Due to the large statistics of isobaric collisions, the differences between the two collision systems can be measured with high precision. Previous studies have proposed that the differences in multiplicity and mean transverse momentum between the isobaric collisions can be used to probe the neutron skin and the symmetry energy slope parameter [20,47]. These studies also suggested that elliptic flow measurements can

*haojiexu@zjhu.edu.cn
†huichaosong@pku.edu.cn

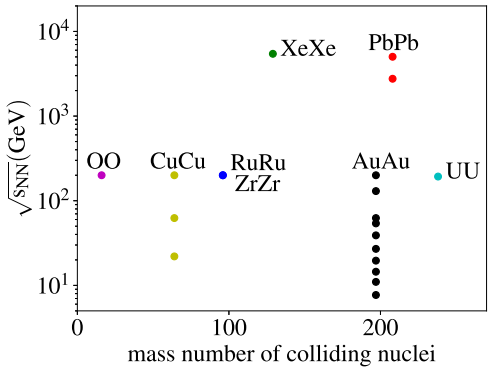

FIG. 1. Different symmetric collision systems at RHIC and the LHC.

also determine the proper nuclear structures of the isobaric nuclei [21,48].

Because of the advantages of isobaric collisions, one might expect using such a method to determine the neutron skin of the benchmark nuclei ^{208}Pb with the rich soft data from Pb + Pb collisions at the LHC [32,49]. Currently, no suitable isobaric partner for ^{208}Pb has been collided in relativistic heavy ion collisions. Figure 1 summarizes the symmetric collisions systems at RHIC and the LHC. The only existing data for isobaric collisions in relativistic heavy ion collisions are those of the $^{96}_{44}$Ru + $^{96}_{44}$Ru and $^{96}_{40}$Zr + $^{96}_{40}$Zr collisions at the top RHIC energy [45]. If we relax the restriction and consider colliding nuclei with similar baryon numbers, called semi-isobaric, we can discuss the ratio observables in such semi-isobaric collisions. For example, the ratio observables between ^{197}Au + ^{197}Au and ^{238}U + ^{238}U collisions have been used to discuss the effect of nuclear deformation [50]. For the purpose of determining the neutron skin thickness of ^{208}Pb, the nucleus ^{197}Au is a good choice, with a large amount of collision experiment data and small deformation effect [51–54]. In this paper, we calculate the anisotropic flows v_2 and v_3 of ^{197}Au + ^{197}Au at $\sqrt{s_{NN}} = 200$ GeV and ^{208}Pb + ^{208}Pb at $\sqrt{s_{NN}} = 2.76$ TeV with different neutron skin sizes and compare them with the measured data of the flow observables. We aim to explore the effect of the neutron skin on the anisotropic flow differences between the semi-isobaric systems.

The paper is organized as follows. Section II gives a brief description of the models and the nuclear density profiles used in this work. Section III discusses the effects of neutron skin on the flow observables in the semi-isobar collisions ^{208}Pb + ^{208}Pb and ^{197}Au + ^{197}Au. Section IV summarizes and concludes this paper.

II. MODEL SETUP

The effect of neutron skin on the final observables in relativistic heavy ion collisions is studied using an IEBE-VISHNU model [55,56]. IEBE-VISHNU [55,56] is a state-of-the-art hybrid model with (2 + 1)-dimensional viscous hydrodynamics [57,58] to describe the expansion of QGP matter, followed by a hadron cascade model (URQMD) to simulate the evolution of the subsequent hadronic matter [59,60]. For more details on the model and parameter setups, please refer to [56,61,62].

TABLE I. The WS parameter for ^{208}Pb and ^{197}Au with different values of the halo-type neutron skin thickness.

$\Delta r_{\rm np}$	^{208}Pb		^{197}Au	
(fm)	R_0 (fm)	a (fm)	R_0 (fm)	a (fm)
0	6.62	0.546	6.38	0.535
0.17	6.62	0.6177	6.38	0.605
0.28	6.62	0.661	6.38	0.647

Here, we implement the TRENTO initial condition model [63] to start the hydrodynamic simulations. The nuclear density in TRENTO is described by a Woods-Saxon (WS) distribution,

$$\rho(r) = \frac{\rho_0}{1 + \exp\left(\frac{r-R}{a_0}\right)}, \tag{1}$$

with

$$R = R_0\left[1 + \beta_2 Y_2^0(\theta,\phi) + \beta_3 Y_3^0(\theta,\phi) + \cdots\right], \tag{2}$$

where ρ_0 is the nuclear saturation density, a is the diffuseness parameter, R_0 is the radius parameter, and β_2 and β_3 are the nuclear deformation parameters. In this study, we set β_n of ^{197}Au and ^{208}Pb to zero because the nuclear deformation parameters are expected to be small for both nuclei.

The nuclear densities can in principle be calculated with some fundamental nuclear structure theories such as energy density functional theory, and the neutron skin is strongly correlated with the symmetry energy slope parameter. For simplicity, we follow the Woods-Saxon framework. The low-energy nuclear experiments indicate that the neutron skin for most of the nuclei is of halo type [64]. The halo-type neutron skin thicknesses of ^{208}Pb and ^{197}Au are constructed by using different diffuseness parameters a for the proton and mass densities, keeping the radius parameter R_0 fixed. The WS parameters for the nuclear mass densities are listed in Table I; the corresponding WS parameters of the proton density are the same as those of the mass density in the case of $\Delta r_{\rm np} = 0$ fm. In this study, we used three sets of neutron skin thicknesses for both Pb and Au, i.e., $\Delta r_{\rm np} = 0$ fm, $\Delta r_{\rm np} =$ 0.17 fm, and $\Delta r_{\rm np} = 0.28$ fm. The $\Delta r_{\rm np} = 0.28$ fm results are taken from the PREX-II experiment for ^{208}Pb nuclei by electroweak parity-violating scattering processes [13]. The $\Delta r_{\rm np} = 0.17$ fm are taken from the STAR measurement for ^{197}Au nuclei by relativistic Au + Au collisions at $\sqrt{s_{NN}} =$ 200 GeV [19].

For the following IEBE-VISHNU simulations for ^{208}Pb + ^{208}Pb collisions at $\sqrt{s_{NN}} = 2.76$ TeV and ^{197}Au + ^{197}Au collisions at $\sqrt{s_{NN}} = 200$ GeV, most of the parameters are taken from a previous Bayesian analysis [65], and are extracted from the spectra and flow data measured in ^{208}Pb + ^{208}Pb collisions at $\sqrt{s_{NN}} = 2.76$ TeV. We use the improved TRENTO version with nucleon constituent scenario; all the model parameters are listed in Table II. Here, we have only changed the normalization factor Norm = 5.35 GeV and the inelastic cross section $\sigma_{NN} = 4.23$ fm^2 [66] for a better description of the soft hadron data in ^{197}Au + ^{197}Au at $\sqrt{s_{NN}} = 200$ GeV at RHIC. We also note that the hydrodynamic parameters are extracted with the $\Delta r_{\rm np} = 0$ fm

TABLE II. The parameters of the IEBE-VISHNU simulations for ^{208}Pb + ^{208}Pb and ^{197}Au + ^{197}Au collisions. The only differences between the two systems are the normalization factor (Norm) and the inelastic cross section (σ_{NN}). All parameters are taken from Ref. [65], except the parameters m and v related to the subnucleon structure.

TRENTO/FREESTREAM		OSU-HYDRO	
Norm	13.94/5.35 GeV	$(\eta/s)_{\rm min}$	0.081
σ_{NN}	6.4/4.23 fm^2	$(\eta/s)_{\rm slope}$	1.11 GeV^{-1}
k	0.1978	$(\eta/s)_{\rm crv}$	−0.48
w	0.956 fm	$(\eta/s)_{\rm hrg}$	0.5
p	0.007	$(\zeta/s)_{\rm max}$	0.052
m	6	$(\zeta/s)_{\rm width}$	0.022 GeV
v	0.956 fm	$(\zeta/s)_{T_{\rm peak}}$	0.183 GeV
$d_{\rm min}$	1.27 fm	$T_{\rm switch}$	0.151 GeV
$\tau_{\rm fs}$	1.16 fm/c		

in the simulations of Pb + Pb collisions; the values should be changed at some levels if the neutron skin effect is included. Since we focus on the ratio observables described by the following Eq. (3) in this study, the main conclusions will not be largely influenced if other hydrodynamic parameters are used.

In order to reduce the systematic uncertainties, we will focus on the ratio of the flow observables between the semi-isobaric systems ^{208}Pb + ^{208}Pb at $\sqrt{s_{NN}} = 2760$ GeV and ^{197}Au + ^{197}Au at $\sqrt{s_{NN}} = 200$ GeV, which is defined as

$$R(X) \equiv \frac{X^{\rm PbPb}}{X^{\rm AuAu}}, \tag{3}$$

Here, the flow observables $v_2\{2\}$, $v_2\{4\}$, and $v_3\{2\}$ are calculated by the standard Q-cumulant methods [67]. The results are compared with the RHIC and LHC data [51–53,68], and only the statistical uncertainties are considered for the data-to-model comparisons.

III. RESULT AND DISCUSSION

Figure 2(a) shows the mean multiplicity as a function of centrality for ^{197}Au + ^{197}Au collisions at $\sqrt{s_{NN}} = 200$ GeV and ^{208}Pb + ^{208}Pb collisions at $\sqrt{s_{NN}} = 2.76$ TeV, calculated from IEBE-VISHNU simulations with different sizes of neutron skin thickness. It demonstrates that the effect of the neutron skin on the mean multiplicity is considerably small, even for the ratios in the semi-isobaric collisions as shown in panel (b). Previous studies in exactly isobaric collisions with high statistics indicate that the mean multiplicities are sensitive to the neutron skin thicknesses and thus to the symmetry energy slope parameter [20,48]. However, the effect is only less than 1% in most-central isobaric collisions; it is invisible in this study with current statistics, and is marginally different at peripheral collisions. We note that the uncertainties from the normalization factor cannot be eliminated for $R(\langle N_{\rm ch}\rangle)$, since we are dealing with the collision system at different collision energies. Therefore, the multiplicity ratio is not a good observable to discuss the neutron skin effect in such semi-isobaric collisions, and the mean transverse momentum $\langle p_T\rangle$ has a similar issue. Therefore, exactly isobaric collisions for ^{208}Pb and/or ^{197}Au are desired to demonstrate the effects.

The halo-type neutron skin is expected to give opposite contributions to v_2 and v_3 in noncentral relativistic heavy ion collisions [21,48]. Figure 3 shows the effect of the neutron skin on v_2 and v_3 in semi-isobaric collisions. Results from hydrodynamic simulations without neutron skin contributions work well for $v_2\{2\}$ and $v_2\{4\}$ in both Pb + Pb and Au + Au collisions, but are underestimated for $v_3\{2\}$. These results are consistent with the previous Bayesian simulations [65]. For the results with thick neutron skin contributions $\Delta r_{\rm np} = 0.28$ fm, the predictions for $v_3\{2\}$ become better, but the $v_2\{2\}$ and $v_2\{4\}$ data are underestimated. Here, we did not change the previous parameters [65] obtained from Bayesian analysis to further improve the description of individual flow harmonics, but the results indicate that the predictions of flow observables from hydrodynamic simulations can be improved by considering the effect of neutron skin thickness.

Figure 4 shows the ratios of $v_2\{2\}/v_3\{2\}$ and $v_2\{4\}/v_3\{2\}$ in both Au + Au collisions and Pb + Pb collisions. The geometry and fluctuations of the diffuseness parameter a are crucial for the simulation of the flow observables in relativistic heavy ion collisions [48,69]. In general, the differences in a between charge and mass densities are mostly due to the halo-type

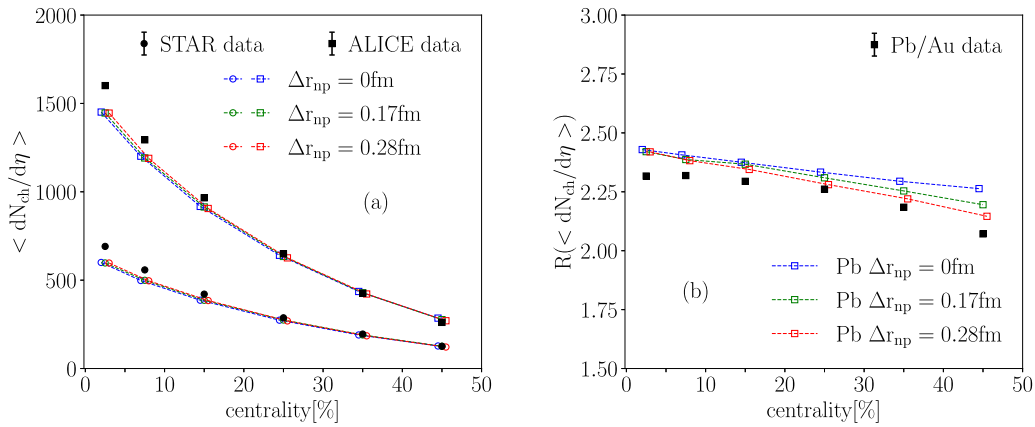

FIG. 2. Charged particle production with different sizes of neutron skin in (a) ^{208}Pb + ^{208}Pb collisions at $\sqrt{s_{NN}} = 2.76$ TeV and ^{197}Au + ^{197}Au collisions at $\sqrt{s_{NN}} = 200$ GeV, and (b) their ratios.

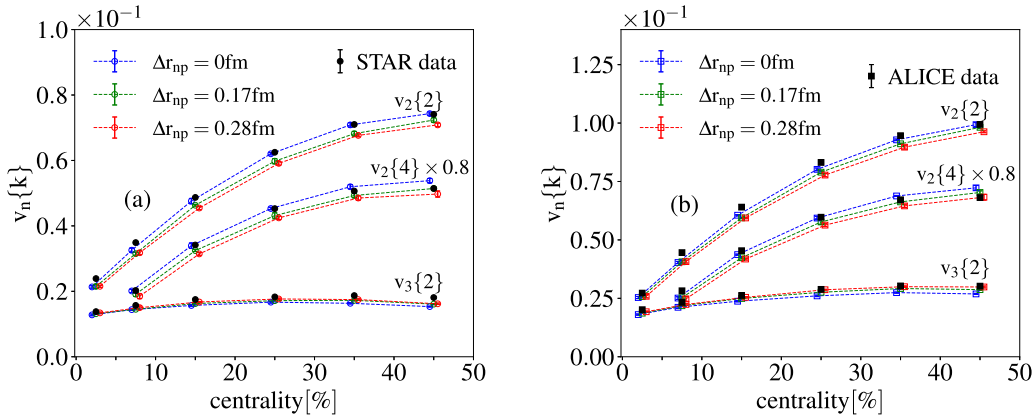

FIG. 3. Flow harmonics $v_2\{2\}$, $v_2\{4\}$, and $v_3\{2\}$ in Pb + Pb collisions at $\sqrt{s_{NN}} = 2.76$ TeV and Au + Au collisions at $\sqrt{s_{NN}} = 200$ GeV, calculated from IEBE-VISHNU hydrodynamic simulations with different sizes of neutron skin for the colliding nuclei.

neutron skin thickness in nuclear structure theory calculations. For most of the central collisions, the ratios of $v_2\{4\}/v_2\{2\}$ are smaller in Au + Au collisions than in Pb + Pb collisions (not shown), indicating that the fluctuation contributions are larger in Au + Au collisions than in Pb + Pb collisions because the system size is smaller in Au + Au collisions with smaller mass number. The differences between the predictions with different sizes of the neutron skin become even more obvious due to the opposite contributions at $v_2\{2\}$ ($v_2\{4\}$) and $v_3\{2\}$. With the current parameter set, the ratio observables from most-central to semicentral collisions can be well explained by the hydrodynamic simulations with a neutron skin of $\Delta r_{\rm np} = 0.17$ fm for both ^{208}Pb and ^{197}Au. This value of $\Delta r_{\rm np}$ is only indicative, as we now proceed to explain.

The individual flow observables are also sensitive to the bulk properties of the QGP medium. The ratios of flow observables in a single collision system discussed above can reduce the systematic uncertainties and the uncertainties from bulk evolution to some extent. However, this cancellation in a single collision system is not good enough. For example, we have checked that the observables discussed above are sensitive to the Gaussian smearing parameter w in the initial TRENTO simulations. To further reduce or eliminate these uncertainties, one can study the flow observables in two collision systems with similar system size and collision energy, as has been done for isobaric $^{96}_{44}$Ru + $^{96}_{44}$Ru and $^{96}_{40}$Zr + $^{96}_{40}$Zr collisions. Here we use Pb + Pb collisions and Au + Au collisions discussed above as semi-isobaric collisions, regardless of the differences in system size and collision energy. Since the observables at top RHIC and LHC energies can be described by the hydrodynamical simulations with a fixed set of parameters [70], the uncertainties from the bulk properties would be small. For example, we have checked that a 20% difference in the free-streaming time τ_f between RHIC and LHC energies will not change our conclusion. Of course, it is expected that the uncertainties can be further reduced when the data of the two systems at the same collision energy can be produced in the future.

Figure 5(a) shows the individual flow ratios $R(v_2\{2\})$, $R(v_2\{4\})$, and $R(v_3\{2\})$, in the semi-isobaric collisions. Here we have fixed the neutron skin for Au with $\Delta r_{\rm np} = 0.17$ fm and changed the neutron skin for Pb. A larger neutron skin in Pb gives larger negative contributions to $v_2\{2\}$ and $v_2\{4\}$, but a positive contribution to $v_3\{2\}$. The results with different sizes of the neutron skin can be distinguished in the ratios of the individual flows, while the uncertainties are large for

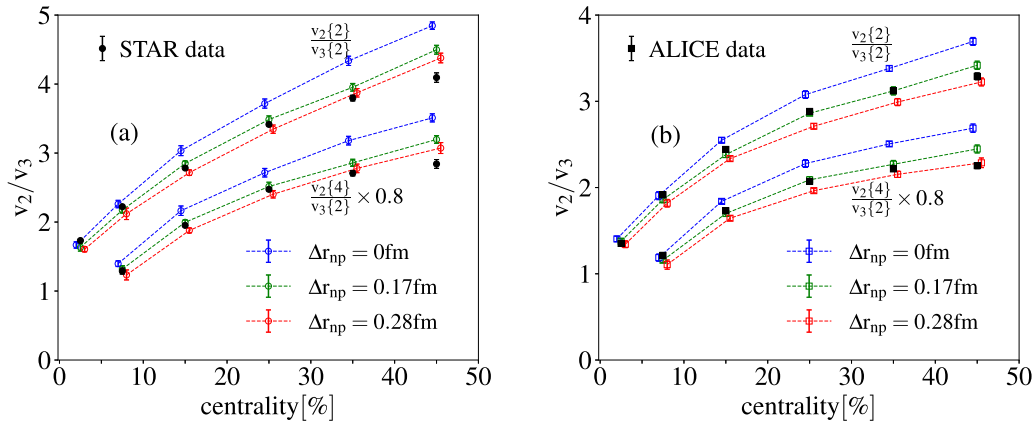

FIG. 4. The flow ratios of $v_2\{2\}/v_3\{2\}$ and $v_2\{4\}/v_3\{2\}$ in (a) Au + Au collisions at $\sqrt{s_{NN}} = 200$ GeV and (b) Pb + Pb collisions at $\sqrt{s_{NN}} = 2.76$ TeV from IEBE-VISHNU hydrodynamic simulations with different sizes of neutron skin for the colliding nuclei.

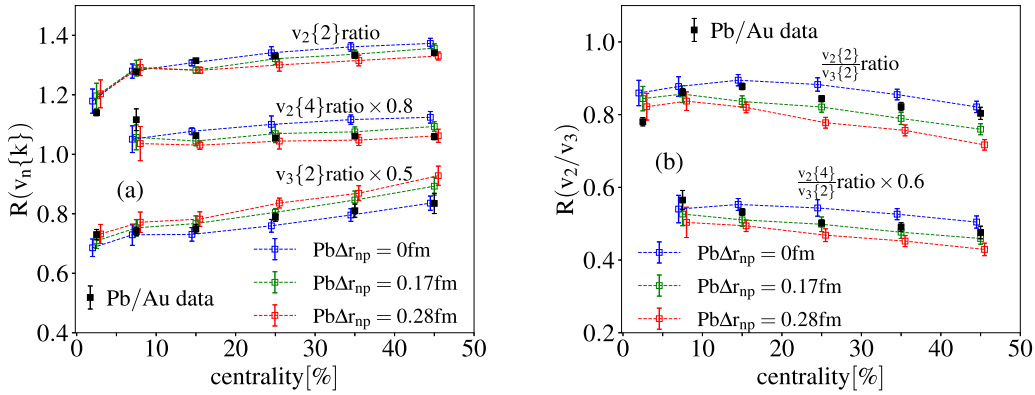

FIG. 5. The ratios of (a) individual flow observables $v_2\{2\}$, $v_2\{4\}$, $v_3\{2\}$ and (b) their double ratios in semi-isobaric collisions, calculated from IEBE-VISHNU hydrodynamic simulations with different sizes of neutron skin for the ^{208}Pb nuclei. The neutrons skin for ^{197}Au is fixed to $\Delta r_{\rm np} = 0.17$ fm.

the model study with current statistics. The double ratios of $R(v_2\{2\}/v_3\{2\})$ and $R(v_2\{4\}/v_3\{2\})$ can be used to enhance the significance of the differences. The results shown in Fig. 5(b) indicate that the experimental data can be well described if Pb has the same size of neutron skin. Here we have fixed the neutron skin for Au with $\Delta r_{\rm np} = 0.17$ fm and changed the neutron skin of Pb. One would expect the same conclusions if the neutron skin of Pb is fixed and the neutron skin of Au is tuned.

We have shown that the neutron skin thickness can be extracted from the flow ratio observables in relativistic semi-isobaric collisions when the neutron skin of the partner nuclei is known. In the more general case, the neutron skin thicknesses of both partner nuclei are unknown. The semi-isobaric collision can be used to study the relative differences between the two nuclei. We find that if the Pb and Au nuclei have the same magnitude of neutron skin thickness, the conclusions from the double ratio flow observations do not change regardless of the exact value of the neutron skin chosen. Such a scaling behavior is shown in Fig. 6. All predictions follow the same trend when ^{197}Au and ^{208}Pb have the same size of neutron skin. Based on this scaling law, the large difference in neutron skin thickness between ^{208}Pb and ^{197}Au measured by the PREX-II and STAR Collaborations is disfavored by measured flow observables and our calculations, indicating that semi-isobaric collisions can provide some tight constraints on the neutron skin thickness and thus the nuclear symmetry energy at relativistic collision energy.

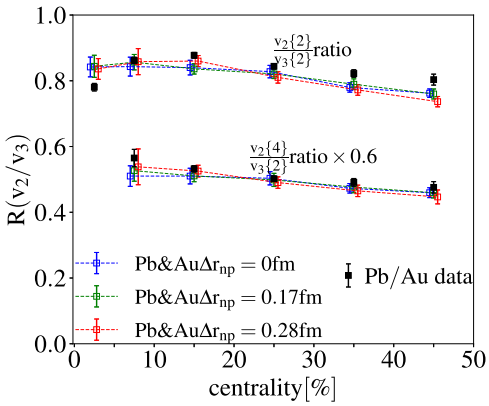

FIG. 6. The approximate scaling law in the isobaric ratio of $v_2\{2\}$, $v_2\{4\}$, $v_3\{2\}$, $v_2\{2\}/v_3\{2\}$, $v_2\{4\}/v_3\{2\}$ when ^{208}Pb and ^{197}Au have the same neutron skin size.

IV. CONCLUSION

This paper focuses on studying the effect of the neutron skin from the flow observables measured in $^{208}\text{Pb}+{}^{208}\text{Pb}$ and $^{197}\text{Au}+{}^{197}\text{Au}$ collisions. Within the framework of IEBE-VISHNU hydrodynamic simulations, the neutron skin thickness is introduced into the Woods-Saxon distribution of ^{208}Pb and ^{197}Au nuclei in the TRENTO initial condition. Using $\Delta r_{\rm np} = 0.17$ fm extracted from $\rho^0 \to \pi^+\pi^-$ photoproduction in ultra-peripheral Au + Au collisions, IEBE-VISHNU can roughly describe the flow data in $^{197}\text{Au}+{}^{197}\text{Au}$ collisions at $\sqrt{s_{NN}} = 200$ GeV, together with the standard hydrodynamic parameters obtained from earlier Bayesian analysis and an appropriate tuned normalization factor for initial entropy at top RHIC energy. Meanwhile, it demonstrates that larger neutron skin suppress the elliptic flow but increases the triangular flow at both RHIC and LHC energies. In order to partially remove the uncertainties from the bulk evolutions, we also calculated the flow ratios $v_2\{2\}/v_3\{2\}$ and $v_2\{4\}/v_3\{2\}$ and found that these two ratios in both Pb + Pb and Au + Au collisions can be well described by the hydrodynamics calculated with $\Delta r_{\rm np} = 0.17$ fm for both ^{208}Pb and ^{197}Au nuclei.

To further investigate the effect of the neutron skin on the flow observables with less systematic uncertainty, we assumed the $^{208}\text{Pb}+{}^{208}\text{Pb}$ collisions at LHC energy and the $^{197}\text{Au}+{}^{197}\text{Au}$ collisions at top RHIC energy as semi-isobaric systems and calculated the flow ratio observables in such semi-isobaric collisions, despite the difference in collision energy and mass number. The associated flow ratios $R(v_2\{2\}/v_3\{2\})$ and $R(v_2\{4\}/v_3\{2\})$ between Au + Au and Pb + Pb collisions suggest that ^{208}Pb and ^{197}Au should have the same magnitude of neutron skin thickness. Thus, the large difference in neutron skin thickness between ^{208}Pb and ^{197}Au measured by the PREX-II and STAR Collaborations is

disfavored by the flow data and our calculations in Au + Au and Pb + Pb collisions. In short, similarly to the exactly isobaric collisions with $^{96}_{44}$Ru + $^{96}_{44}$Ru and $^{96}_{40}$Zr + $^{96}_{40}$Zr at the same collision energy, the semi-isobaric collisions proposed in this study can also give constraints on the neutron skin thickness and symmetry energy slope parameters in an unconventional way with a set of the existing flow data.

ACKNOWLEDGMENTS

This work is supported in part by the National Natural Science Foundation of China under Grants No. 12247107 and No. 12075007. H.J.X. is supported by the National Natural Science Foundation of China under Grants No. 12275082, No. 12035006, No. 12075085, and No. 12147101.

[1] B. A. Brown, Phys. Rev. Lett. **85**, 5296 (2000).
[2] C. J. Horowitz and J. Piekarewicz, Phys. Rev. Lett. **86**, 5647 (2001).
[3] B.-A. Li, L.-W. Chen, and C. M. Ko, Phys. Rep. **464**, 113 (2008).
[4] L.-W. Chen, C. M. Ko, B.-A. Li, and J. Xu, Phys. Rev. C **82**, 024321 (2010).
[5] J. Bartel, P. Quentin, M. Brack, C. Guet, and H. B. Hakansson, Nucl. Phys. A **386**, 79 (1982).
[6] R. Machleidt, Adv. Nucl. Phys. **19**, 189 (1989).
[7] B. A. Brown, Phys. Rev. C **58**, 220 (1998).
[8] R. J. Furnstahl, Nucl. Phys. A **706**, 85 (2002).
[9] L.-W. Chen, C. M. Ko, and B.-A. Li, Phys. Rev. C **72**, 064309 (2005).
[10] X. Roca-Maza, M. Centelles, X. Vinas, and M. Warda, Phys. Rev. Lett. **106**, 252501 (2011).
[11] M. B. Tsang, J. R. Stone, F. Camera, P. Danielewicz, S. Gandolfi, K. Hebeler, C. J. Horowitz, Jenny Lee, W. G. Lynch, Z. Kohley *et al.*, Phys. Rev. C **86**, 015803 (2012).
[12] C. J. Horowitz, E. F. Brown, Y. Kim, W. G. Lynch, R. Michaels, A. Ono, J. Piekarewicz, M. B. Tsang, and H. H. Wolter, J. Phys. G **41**, 093001 (2014).
[13] D. Adhikari *et al.* (PREX Collaboration), Phys. Rev. Lett. **126**, 172502 (2021).
[14] D. Adhikari *et al.* (CREX Collaboration), Phys. Rev. Lett. **129**, 042501 (2022).
[15] B. T. Reed, F. J. Fattoyev, C. J. Horowitz, and J. Piekarewicz, Phys. Rev. Lett. **126**, 172503 (2021).
[16] E. Yüksel and N. Paar, Phys. Lett. B **836**, 137622 (2023).
[17] Z. Zhang and L.-W. Chen, Phys. Rev. C **108**, 024317 (2023).
[18] H. Alvensleben, U. Becker, W. K. Bertram, M. Chen, K. J. Cohen, T. M. Knasel, R. Marshall, D. J. Quinn, M. Rohde, G. H. Sanders *et al.*, Phys. Rev. Lett. **24**, 786 (1970).
[19] M. Abdallah *et al.* (STAR Collaboration), Sci. Adv. **9**, eabq3903 (2023).
[20] H. Li, H.-j. Xu, Y. Zhou, X. Wang, J. Zhao, L.-W. Chen, and F. Wang, Phys. Rev. Lett. **125**, 222301 (2020).
[21] C. Zhang and J. Jia, Phys. Rev. Lett. **128**, 022301 (2022).
[22] G. Nijs and W. van der Schee, SciPost Phys. **15**, 041 (2023).
[23] J. Jia, G. Giacalone, and C. Zhang, Phys. Rev. Lett. **131**, 022301 (2023).
[24] C. Zhang, S. Bhatta, and J. Jia, Phys. Rev. C **106**, L031901 (2022).
[25] M. Nie, C. Zhang, Z. Chen, L. Yi, and J. Jia, Phys. Lett. B **845**, 138177 (2023).
[26] B.-S. Xi, X.-G. Deng, S. Zhang, and Y.-G. Ma, Eur. Phys. J. A **59**, 33 (2023).
[27] Y.-L. Cheng, S. Shi, Y.-G. Ma, H. Stöcker, and K. Zhou, Phys. Rev. C **107**, 064909 (2023).
[28] W. van der Schee, Y.-J. Lee, G. Nijs, and Y. Chen, arXiv:2307.11836 [nucl-th].
[29] G. Giacalone, G. Nijs, and W. van der Schee, Phys. Rev. Lett. **131**, 202302 (2023).
[30] J. Adams *et al.* (STAR Collaboration), Nucl. Phys. A **757**, 102 (2005).
[31] K. Adcox *et al.* (PHENIX Collaboration), Nucl. Phys. A **757**, 184 (2005).
[32] K. Aamodt *et al.* (ALICE Collaboration), Phys. Rev. Lett. **105**, 252302 (2010).
[33] M. Gyulassy, I. Vitev, X.-N. Wang, and B.-W. Zhang, in *Quark-Gluon Plasma 3*, edited by R. C. Hwa (World Scientific, Singapore, 2003), p. 123.
[34] B. Müller, J. Schukraft, and B. Wyslouch, Annu. Rev. Nucl. Part. Sci. **62**, 361 (2012).
[35] H. Song, S. A. Bass, U. Heinz, T. Hirano, and C. Shen, Phys. Rev. Lett. **106**, 192301 (2011); **109**, 139904(E) (2012).
[36] C. Gale, S. Jeon, and B. Schenke, Int. J. Mod. Phys. A **28**, 1340011 (2013).
[37] H. Song, Pramana **84**, 703 (2015).
[38] U. Heinz and R. Snellings, Annu. Rev. Nucl. Part. Sci. **63**, 123 (2013).
[39] H. Song, Y. Zhou, and K. Gajdosova, Nucl. Sci. Tech. **28**, 99 (2017).
[40] D. Everett *et al.* (JETSCAPE Collaboration), Phys. Rev. C **103**, 054904 (2021).
[41] D. Everett *et al.* (JETSCAPE Collaboration), Phys. Rev. Lett. **126**, 242301 (2021).
[42] J.-Y. Ollitrault, Phys. Rev. D **46**, 229 (1992).
[43] B. Bally, J. D. Brandenburg, G. Giacalone, U. Heinz, S. Huang, J. Jia, D. Lee, Y.-J. Lee, W. Li, C. Loizides *et al.*, arXiv:2209.11042.
[44] H.-J. Xu, X. Wang, H. Li, J. Zhao, Z.-W. Lin, C. Shen, and F. Wang, Phys. Rev. Lett. **121**, 022301 (2018).
[45] M. Abdallah *et al.* (STAR Collaboration), Phys. Rev. C **105**, 014901 (2022).
[46] H.-j. Xu, H. Li, Y. Zhou, X. Wang, J. Zhao, L.-W. Chen, and F. Wang, Phys. Rev. C **105**, L011901(R) (2022).
[47] H.-j. Xu, W. Zhao, H. Li, Y. Zhou, L.-W. Chen, and F. Wang, Phys. Rev. C **108**, L011902 (2023).
[48] H.-j. Xu, H. Li, X. Wang, C. Shen, and F. Wang, Phys. Lett. B **819**, 136453 (2021).
[49] B. Abelev *et al.* (ALICE Collaboration), Phys. Lett. B **719**, 29 (2013).
[50] J. Jia, S. Huang, and C. Zhang, Phys. Rev. C **105**, 014906 (2022).
[51] B. I. Abelev *et al.* (STAR Collaboration), Phys. Rev. C **79**, 034909 (2009).
[52] J. Adams *et al.* (STAR Collaboration), Phys. Rev. C **72**, 014904 (2005).

[53] L. Adamczyk *et al.* (STAR Collaboration), Phys. Rev. C **88**, 014904 (2013).
[54] P. Möller, J. R. Nix, W. D. Myers, and W. J. Swiatecki, Atom. Data Nucl. Data Tabl. **59**, 185 (1995).
[55] H. Song, S. A. Bass, and U. Heinz, Phys. Rev. C **83**, 024912 (2011).
[56] C. Shen, Z. Qiu, H. Song, J. Bernhard, S. Bass, and U. Heinz, Comput. Phys. Commun. **199**, 61 (2016).
[57] H. Song and U. Heinz, Phys. Rev. C **77**, 064901 (2008).
[58] H. Song and U. Heinz, Phys. Lett. B **658**, 279 (2008).
[59] S. A. Bass, M. Belkacem, M. Bleicher, M. Brandstetter, L. Bravina, C. Ernst, L. Gerland, M. Hofmann, S. Hofmann, J. Konopka *et al.*, Prog. Part. Nucl. Phys. **41**, 255 (1998).
[60] M. Bleicher, E. Zabrodin, C. Spieles, S. A. Bass, C. Ernst, S. Soff, L. Bravina, M. Belkacem, H. Weber, H. Stöcker *et al.*, J. Phys. G **25**, 1859 (1999).
[61] H.-j. Xu, Z. Li, and H. Song, Phys. Rev. C **93**, 064905 (2016).
[62] W. Zhao, H.-j. Xu, and H. Song, Eur. Phys. J. C **77**, 645 (2017).
[63] J. S. Moreland, J. E. Bernhard, and S. A. Bass, Phys. Rev. C **92**, 011901(R) (2015).
[64] A. Trzcińska, J. Jastrzębski, P. Lubiński, F. J. Hartmann, R. Schmidt, T. von Egidy, and B. Klos, Phys. Rev. Lett. **87**, 082501 (2001).
[65] J. E. Bernhard, J. S. Moreland, and S. A. Bass, Nat. Phys. **15**, 1113 (2019).
[66] A. Adare *et al.* (PHENIX Collaboration), Phys. Rev. C **93**, 024901 (2016).
[67] A. Bilandzic, R. Snellings, and S. Voloshin, Phys. Rev. C **83**, 044913 (2011).
[68] J. Adam *et al.* (ALICE Collaboration), Phys. Rev. Lett. **116**, 132302 (2016).
[69] J.-f. Wang, H.-j. Xu, and F. Wang, arXiv:2305.17114.
[70] B. Schenke, C. Shen, and P. Tribedy, Phys. Rev. C **102**, 044905 (2020).